

Theory of Stellar Oscillations

Margarida S. Cunha

Abstract In recent years, astronomers have witnessed major progresses in the field of stellar physics. This was made possible thanks to the combination of a solid theoretical understanding of the phenomena of stellar pulsations and the availability of a tremendous amount of exquisite space-based asteroseismic data. In this context, this chapter reviews the basic theory of stellar pulsations, considering small, adiabatic perturbations to a static, spherically symmetric equilibrium. It starts with a brief discussion of the solar oscillation spectrum, followed by the setting of the theoretical problem, including the presentation of the equations of hydrodynamics, their perturbation, and a discussion of the functional form of the solutions. Emphasis is put on the physical properties of the different types of modes, in particular acoustic (p-) and gravity (g-) modes and their propagation cavities. The surface (f-) mode solutions are also discussed. While not attempting to be comprehensive, it is hoped that the summary presented in this chapter addresses the most important theoretical aspects that are required for a solid start in stellar pulsations research.

1 Introduction

The study of stellar pulsations is revolutionizing our knowledge of the internal structure and dynamics of stars and, as a consequence, also our understanding of stellar evolution. This is made possible through the combination of a solid theoretical understanding of the phenomena of stellar pulsations and the availability of a tremendous amount of high-quality data, in particular that acquired from space with satellites such as *SOHO* (Domingo et al. 1995), observing the Sun for over 20 years, and *CoRoT* (Baglin et al. 2006) and *Kepler* (Gilliland et al. 2010; Koch et al. 2010).

In this chapter I review basic aspects of the theory of stellar pulsations. Given the limited space available, options had to be made on what to discuss. A more detailed

M.S. Cunha (✉)

Instituto de Astrofísica e Ciências do Espaço, Universidade do Porto, CAUP, Rua das Estrelas,
4150-762 Porto, Portugal

e-mail: mcunha@astro.up.pt

© Springer International Publishing AG 2018

T.L. Campante et al. (eds.), *Asteroseismology and Exoplanets: Listening to the Stars and Searching for New Worlds*, Astrophysics and Space Science Proceedings 49, DOI 10.1007/978-3-319-59315-9_2

27

view of the aspects considered here, as well as discussions of the issues that have been left out can be found, e.g., in published books (Unno et al. 1989; Aerts et al. 2010), lecture notes (Gough 1993), as well as in other long reviews (Cunha et al. 2007; Basu 2016).

While this chapter is dedicated to the theory of stellar pulsations, it is interesting and motivating to start by inspecting one of the main observational results in this context, namely, the oscillation power density spectrum of the Sun. This is shown in the upper panel of Fig. 1. The first aspect that catches the eye is that the oscillation spectrum is composed of a number of discrete frequencies, whose power is modulated over frequency, showing a close to Gaussian shape. This is typical of oscillation spectra of solar-like pulsators in which modes are intrinsically stable (meaning that small perturbations are damped) and continuously excited

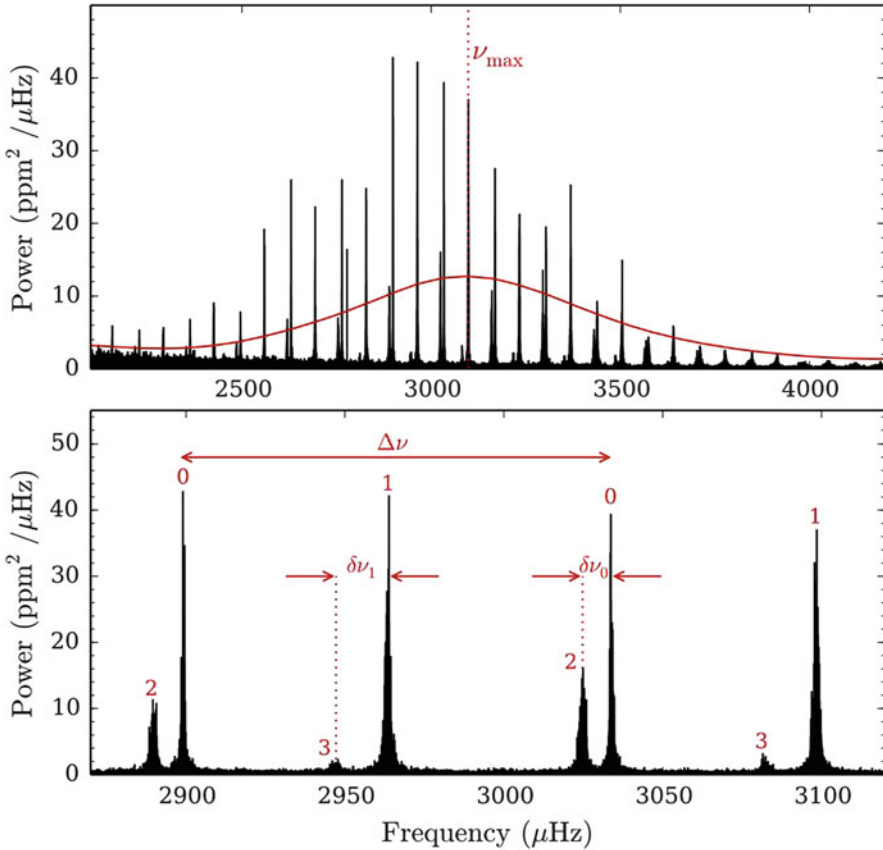


Fig. 1 Power density spectrum of the Sun obtained from data acquired with VIRGO/SPM onboard the *SOHO* satellite (Fröhlich et al. 1995; Jiménez et al. 2002). *Top*: The red line shows the power spectrum density smoothed by $3\Delta\nu$ and multiplied by 50, used to estimate ν_{\max} . *Bottom*: A zoom of the upper panel illustrating a few modes, identified by mode degree. The large frequency separation, $\Delta\nu$, and the small frequency separations between pairs of modes with degrees $l = 0, 2$, $\delta\nu_0$, and pairs of modes with degrees $l = 1, 3$, $\delta\nu_1$, are also shown (figure courtesy of A. Santos)

stochastically by convection. Other stellar pulsators, in which oscillations are intrinsically unstable, with small perturbations growing due to some sort of coherent excitation mechanism, will still show oscillation spectra composed of discrete frequencies, but often a less regular pattern as a consequence of not all possible frequencies being excited or observed. An important observable for solar-like pulsators is the frequency of maximum power, ν_{\max} , shown in Fig. 1. There are different approaches to derive it (Verner et al. 2011, and references therein) that usually involve considering a heavily-smoothed version of the oscillation power spectrum.

The lower panel of Fig. 1 shows a close-up of the regular peak structure seen in the upper panel. Here each mode is identified by a positive integer, the mode degree, which will be discussed in detail in Sect. 2.3. Two main separations are identified in the figure, namely, the large separation, $\Delta\nu$, between consecutive modes of the same degree and the small separation, $\delta\nu$, between modes of similar frequency and degree differing by two.

The large separation has been shown to scale as $\Delta\nu \propto \sqrt{\bar{\rho}}$ (Tassoul 1980), where $\bar{\rho}$ is the mean density of the star. Moreover, the frequency of maximum power has been suggested to scale with the surface gravity and effective temperature as $\nu_{\max} \propto g T_{\text{eff}}^{-1/2}$ (Brown et al. 1991; Kjeldsen and Bedding 1995). Together, these scaling relations provide two equations that can be used for a first estimate of the stellar mass and radius, once the effective temperature is known, namely,

$$\begin{aligned} \frac{R}{R_{\odot}} &\approx \left(\frac{\nu_{\max}}{\nu_{\max,\odot}} \right) \left(\frac{\overline{\Delta\nu}}{\overline{\Delta\nu_{\odot}}} \right)^{-2} \left(\frac{T_{\text{eff}}}{T_{\text{eff},\odot}} \right)^{1/2}, \\ \frac{M}{M_{\odot}} &\approx \left(\frac{\nu_{\max}}{\nu_{\max,\odot}} \right)^3 \left(\frac{\overline{\Delta\nu}}{\overline{\Delta\nu_{\odot}}} \right)^{-4} \left(\frac{T_{\text{eff}}}{T_{\text{eff},\odot}} \right)^{3/2}, \end{aligned} \quad (1)$$

where the overbar stands for a suitable average taken over the different pairs of modes and solar values are marked by the index ‘ \odot ’.

Finally, the small separation depends strongly on the sound speed in the stellar core and is, thus, very sensitive to stellar age. These quantities shall be discussed further in Sect. 5. Before that, I will introduce the pulsation equations in Sect. 2, and discuss the corresponding solutions in Sects. 3–4.

2 Equations for Linear, Adiabatic Stellar Pulsations

In this section I set the problem of linear, adiabatic stellar pulsations. I start from the equations of hydrodynamics for an inviscid fluid and then consider small, adiabatic perturbations about a spherically symmetric, static equilibrium. Finally, I discuss the functional form of the solutions on the sphere and the boundary conditions.

Let us assume that a gas can be treated as a continuum with thermodynamic properties well defined at each position in space, \mathbf{r} . Let f be a scalar property of the gas. There are two ways of looking at the time evolution of f : (1) at fixed position

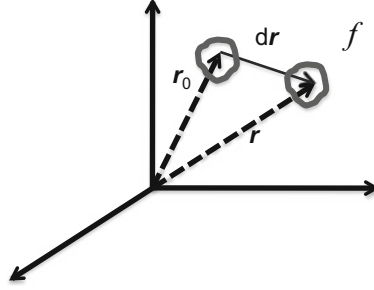


Fig. 2 Eulerian versus Lagrangian descriptions. In the Eulerian description the evolution of the property, f , of the gas is considered at fixed position, \mathbf{r}_0 , by comparing $f(\mathbf{r}_0, t_0)$ with $f(\mathbf{r}_0, t_1)$, while in the Lagrangian description the evolution is considered following the motion by comparing $f(\mathbf{r}_0, t_0)$ with $f(\mathbf{r}, t_1)$

\mathbf{r}_0 and (2) following the motion (see Fig. 2). The first corresponds to an Eulerian description and the second to a Lagrangian description. Both perspectives are useful and commonly used in the study of stellar pulsations. The two descriptions are related by

$$\frac{df}{dt} = \frac{\partial f}{\partial t} + \nabla f \cdot \frac{d\mathbf{r}}{dt} \equiv \frac{\partial f}{\partial t} + \mathbf{v} \cdot \nabla f, \quad (2)$$

where \mathbf{v} is the velocity, d/dt is the time derivative following the motion (Lagrangian description) and $\partial/\partial t$ is the time derivative at fixed position (Eulerian description). Likewise, for a vector quantity, \mathbf{F} , the two derivatives are related by

$$\frac{d\mathbf{F}}{dt} = \frac{\partial \mathbf{F}}{\partial t} + (\mathbf{v} \cdot \nabla) \mathbf{F}. \quad (3)$$

2.1 The Conservation Laws

The evolution of the properties of a fluid is described by a set of equations that translate conservation laws. In what follows these equations are summarized under particular conditions that will be discussed below. Conservation of mass, linear momentum, and energy are expressed, respectively, by

$$\begin{aligned} \frac{d\rho}{dt} &= -\rho \nabla \cdot \mathbf{v}, \\ \rho \frac{d\mathbf{v}}{dt} &= -\nabla p + \rho \mathbf{g} + \mathbf{F}_{\text{oth}}, \\ \frac{dq}{dt} &= \frac{dE}{dt} + p \frac{d(1/\rho)}{dt}, \end{aligned} \quad (4)$$

where ρ and p are, respectively, the fluid density and pressure, \mathbf{g} is the acceleration of gravity, \mathbf{F}_{oth} are other body forces, expressed per unit volume, that may act on the fluid, besides gravity (e.g., the Lorentz force, if a magnetic field is present), and E and q are, respectively, the internal energy and heat supplied to the system, both per unit mass.

The first of these equations, known as the continuity equation, expresses that the rate of change of the mass within a given volume must equal, with opposite sign, the mass crossing the surface that encloses that volume, per unit time. The second, the equation of motion, expresses that the change in linear momentum of an element of fluid must equal the force acting on it by its surroundings. It is written under the assumption that the fluid is inviscid, which is a good approximation under stellar conditions. The third equation translates the first law of thermodynamics and it states that the change in the internal energy of a system must equal the heat supplied to the system minus the work done by the system on its surroundings. This equation can be written in different forms. A useful one, adopted below, is

$$\frac{dq}{dt} = \frac{1}{\rho(\Gamma_3 - 1)} \left(\frac{dp}{dt} - \frac{\Gamma_1 p}{\rho} \frac{d\rho}{dt} \right), \quad (5)$$

where Γ_1 and Γ_3 are adiabatic exponents defined by the adiabatic derivatives,

$$\Gamma_1 = \left(\frac{\partial \ln p}{\partial \ln \rho} \right)_{\text{ad}}, \quad \Gamma_3 - 1 = \left(\frac{\partial \ln T}{\partial \ln \rho} \right)_{\text{ad}}, \quad (6)$$

and T is the temperature of the fluid. From Eq.(5) one can further define the adiabatic sound speed, c . Making the left-hand side equal to zero one finds:

$$c^2 \equiv \frac{dp}{d\rho} = \frac{\Gamma_1 p}{\rho}. \quad (7)$$

Finally, it should be noted that the thermodynamic variables T , ρ , and p are not all independent, but rather are related by the equation of state that can be expressed as $\mathcal{F}(T, p, \rho) = 0$, where \mathcal{F} is a function that depends on the conditions of the fluid. Since in this chapter only adiabatic oscillations will be considered, the explicit form of the equation of state will not be needed. However, this equation will still be required if the reader is interested in deriving the temperature fluctuations associated to the perturbations in the density and pressure.

2.2 Perturbative Analysis

Consider an equilibrium state that is: (1) static, meaning that there are no velocities and all derivatives at fixed position are null ($\partial/\partial t = 0$) and (2) spherically

symmetric, implying, e.g., that there is no rotation or magnetic fields. Then, in the equilibrium, one has:

$$\nabla p_0 = \rho_0 \mathbf{g}_0 \equiv -\rho_0 g_0 \hat{\mathbf{a}}_r, \quad (8)$$

where the index '0' is used to identify the equilibrium quantities and $\hat{\mathbf{a}}_r$ is the unit vector in the radial direction pointing outwardly from the centre of the star, making the scalar g_0 a positive quantity.

Now let us assume that the equilibrium is perturbed under the following conditions: (1) the perturbations are adiabatic and (2) they are small, in the sense that non-linear terms in the perturbations can be neglected.

The adiabatic condition implies the assumption that no heat is exchanged with the element of fluid during the perturbation, a condition that is very closely satisfied almost everywhere in the star. This can be seen by comparing the characteristic timescales of pulsations, typically found in the range of minutes to a few days, with the timescale for radiation that, except very close to the stellar surface, has characteristic values many orders of magnitude larger than the pulsation period (e.g., exceeding a million years in the Sun, when the Sun is considered as a whole).

Under the above conditions, let f be a scalar property of the gas, and f' and δf be, respectively, the Eulerian and Lagrangian perturbations to it. Then $f = f_0 + f'$ and $\delta f = f' + \boldsymbol{\xi} \cdot \nabla f_0$, where $\boldsymbol{\xi}$ is the displacement vector ($\equiv \mathbf{r} - \mathbf{r}_0$). Moreover, since the perturbations are linear, the velocity of a given element of fluid is

$$\mathbf{v} \equiv \frac{d\boldsymbol{\xi}}{dt} \approx \frac{\partial \boldsymbol{\xi}}{\partial t}. \quad (9)$$

Perturbing the system of equations (4) [with energy conservation expressed as in Eq. (5)], using Eqs. (8) and (9), and integrating in time the equations of continuity and energy, one finds that linear adiabatic perturbations about a static spherically symmetric equilibrium are described by the following set of equations:

$$\begin{aligned} \rho' &= -\nabla \cdot (\rho_0 \boldsymbol{\xi}), \\ \rho_0 \frac{\partial^2 \boldsymbol{\xi}}{\partial t^2} &= -\nabla p' - \rho_0 \nabla \phi' - \rho' \nabla \phi_0, \\ \nabla^2 \phi' &= 4\pi G \rho', \\ p' + \boldsymbol{\xi} \cdot \nabla p_0 &= \frac{\Gamma_{1,0} p_0}{\rho_0} (\rho' + \boldsymbol{\xi} \cdot \nabla \rho_0). \end{aligned} \quad (10)$$

To reach the system of equations above, I have further defined the acceleration of gravity in terms of the gravitational potential ϕ , such that $\mathbf{g} = -\nabla \phi$ and, accordingly, considered in addition the Poisson equation that relates the gravitational potential to the fluid density.

Taking the equilibrium quantities as known, one can identify four variables in the system above (three scalars and one vector), namely ρ' , p' , ϕ' , and $\boldsymbol{\xi}$. These four equations thus form a closed system that can be solved, with adequate boundary conditions.

2.3 Solutions on a Sphere

Consider the spherical coordinate system (r, θ, φ) such that the variables ρ', p', ϕ', ξ are expressed as functions of r, θ, φ and t .

It can be shown by substitution (or derived by the technique of separation of variables) that the system of equations (10) admits solutions of the type

$$\begin{aligned} f'(r, \theta, \varphi, t) &= \Re \left\{ f'(r) Y_l^m(\theta, \varphi) e^{-i\omega t} \right\}, \\ \xi(r, \theta, \varphi, t) &= \Re \left\{ \left[\xi_r(r) Y_l^m(\theta, \varphi) \hat{a}_r + \xi_h(r) \left(\frac{\partial Y_l^m}{\partial \theta} \hat{a}_\theta + \frac{1}{\sin \theta} \frac{\partial Y_l^m}{\partial \varphi} \hat{a}_\varphi \right) \right] e^{-i\omega t} \right\}, \end{aligned} \quad (11)$$

where f' stands for any of the scalar perturbations, ξ_r and ξ_h are, respectively, the depth-dependent amplitudes of the radial and horizontal components of the displacement and \hat{a}_i are the components of the unit vectors of the spherical coordinate system.

The time dependence of the solution is associated to the angular oscillation frequency ω . The sign in the exponential is arbitrary. Here it is chosen to be negative to guarantee that in cases when ω is complex the growth rate (i.e., the imaginary part of the frequency) is positive when the perturbation grows. The possible values of ω are determined by imposing the boundary conditions that shall be discussed later. In practice, since the equations were derived under the assumption that the perturbations are adiabatic, so far as the boundary conditions are fully reflective (i.e., no energy is lost through the boundary), ω is real. That will be the only case discussed in this chapter.

The angular dependence of the solutions is given by the spherical harmonic functions Y_l^m , characterized by the angular degree l (a non-negative integer), and the azimuthal order m , an integer that takes values between $-l$ and l . The angular degree defines the number of surface nodes and the absolute value of the azimuthal order defines the subset of those that cross the equator. This means that $|m|$ defines the orientation of that solution on the sphere, something that will be relevant for the discussion below. An example of low-degree spherical harmonic functions with identified values of l and $|m|$ is shown in Fig. 3. Since $Y_l^m \propto P_l^m(\cos \theta) e^{im\varphi}$, where P_l^m are the associated Legendre functions, the sign of m defines whether the associated solution is travelling eastwardly or westwardly in the chosen reference frame. Given the negative sign adopted for the time-dependent part of the solution the perturbations are found to vary as $e^{i(m\varphi - \omega t)}$. This means that in this case a positive m corresponds to a solution travelling eastwardly. I note, however, that not all literature adopts the same definition, since sometimes the opposite sign is chosen for the exponent in the time-dependent exponential. Finally, from the properties of the spherical harmonics, one has that

$$\nabla_h^2 Y_l^m = -\frac{l(l+1)}{r^2} Y_l^m \equiv -\kappa_h^2 Y_l^m, \quad (12)$$

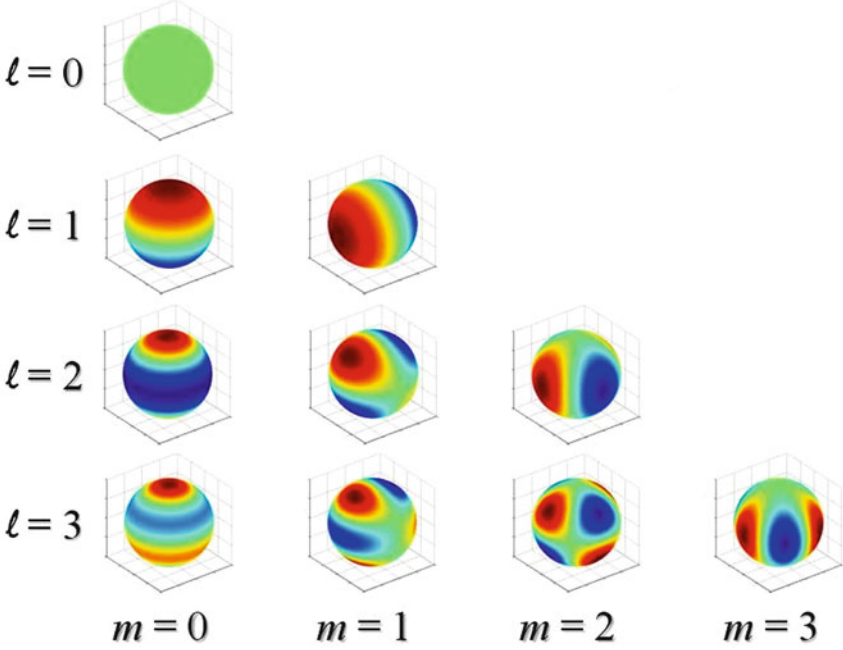


Fig. 3 Examples of spherical harmonic functions, Y_l^m , for mode degrees in the range $l = 0-3$. For each mode degree, all possible non-negative values of m are shown. Red and blue show perturbations of opposite sign

where κ_h has been identified as the horizontal wavenumber of the perturbation when the latter is interpreted, locally, as a plane wave.

The last part of the solutions in Eq. (11) are the radial-dependent amplitudes. For simplicity, radial-dependent parts of scalar perturbations have been named with the same symbol as the full solutions. Using the full solutions separated as in Eq. (11) in the system of equations (10), one can derive a set of equations governing these amplitude functions. After eliminating the horizontal component of the displacement by combining the continuity equation and the horizontal divergence of the perturbed momentum equation, and eliminating the Eulerian perturbation to the density through the adiabatic relation, one finds that the radial-dependent amplitudes $p'(r)$, $\phi'(r)$, and $\xi_r(r)$, obey the following system of equations:

$$\begin{aligned}
 \frac{1}{r^2} \frac{d}{dr} (r^2 \xi_r) - \frac{g_0}{c_0^2} \xi_r - \left(\frac{S_l^2}{\omega^2} - 1 \right) \frac{1}{c_0^2 \rho_0} p' &= \frac{l(l+1)}{r^2 \omega^2} \phi', \\
 \frac{dp'}{dr} + \frac{g_0}{c_0^2} p' - \rho_0 (\omega^2 - N_0^2) \xi_r &= -\rho_0 \frac{d\phi'}{dr}, \\
 \frac{1}{r^2} \frac{d}{dr} \left(r^2 \frac{d\phi'}{dr} \right) - \frac{l(l+1)}{r^2} \phi' &= 4\pi G \left(\frac{p'}{c_0^2} + \frac{\rho_0 N_0^2}{g_0} \xi_r \right), \quad (13)
 \end{aligned}$$

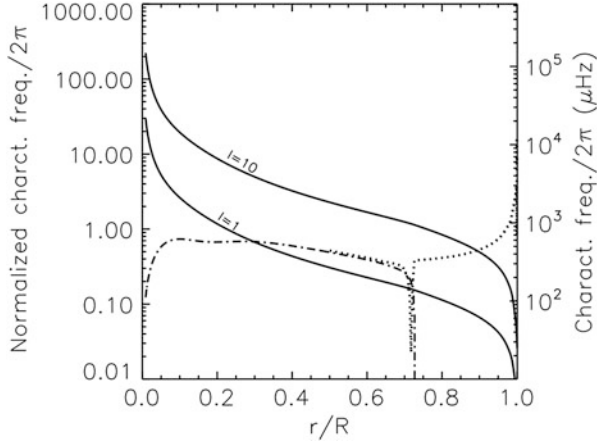


Fig. 4 Lamb frequency, S_l (continuous lines), for $l = 1$ and $l = 10$, buoyancy frequency, N_0 (dashed-dotted line), and critical frequency, ω_c (dotted line), displayed in the outer 50% of the stellar radius only), for a model of the Sun, all divided by 2π . The *left vertical axis* shows dimensionless values of these characteristic frequencies obtained by multiplying them by t_{dyn} . The *right vertical axis* indicates the true physical values

where two characteristic frequencies have been defined: the Lamb frequency, S_l ; and the buoyancy (or Brunt–Väisälä) frequency, N_0 . The squares of these quantities are given, respectively, by

$$S_l^2 = \frac{l(l+1)c_0^2}{r^2}, \quad N_0^2 = g_0 \left[\frac{1}{\Gamma_{1,0}} \frac{d \ln p_0}{dr} - \frac{d \ln \rho_0}{dr} \right]. \quad (14)$$

Examples of the Lamb frequency and buoyancy frequency are shown in Figs. 4 and 5 for a model of the Sun and a model of a star in the red-giant branch, respectively. The buoyancy frequency is seen only where $N^2 > 0$, which marks stellar layers that are stable to convection.

A significant difference is found in the characteristic values of the Lamb frequency in the two stars, as seen by comparing the scales on the right-hand side vertical axes in Figs. 4 and 5. This is because this frequency scales approximately with the inverse of the dynamical timescale of the star, $t_{\text{dyn}} = (R^3/GM)^{1/2}$, hence depending significantly on stellar radii. The vertical scale on the left-hand side of each figure shows the characteristic frequencies in units of $1/t_{\text{dyn}}$, illustrating the similarity of the Lamb frequency in the two stars once the scaling is accounted for. The second aspect that calls attention in these figures is that the buoyancy frequency in the more evolved star shows a much more significant contrast, increasing significantly towards the stellar centre. This is a consequence of the increasing density gradient in the innermost layers as the star evolves and the core contracts. These structural differences between main-sequence and red-giant stars have significant impact on the properties of their oscillations, as will be discussed in Sect. 4.

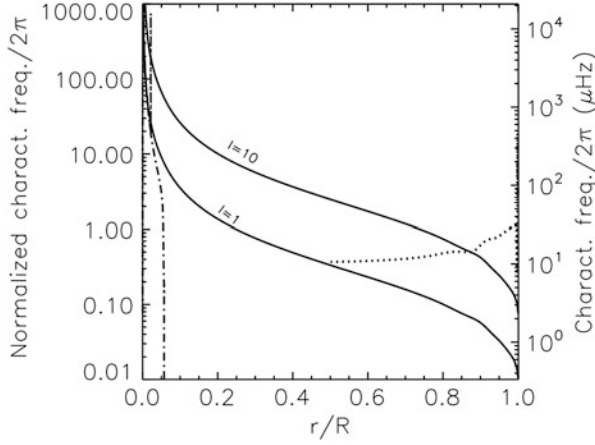


Fig. 5 Same as Fig. 4 but for a model of a star in the red-giant branch

There are a number of points that should be stressed in relation to the system of equations (13):

- First, the system only contains total derivatives, reminding us that the variables are the depth-dependent parts of the solutions only. In fact, the system of equations (13) forms a system of linear, total differential equations of fourth order for four unknown functions, namely, the depth-dependent amplitude functions, ξ_r , p' , ϕ' , and $d\phi'/dr$. We have, thus, at this point, reduced the original 3-dimensional problem into a 1-dimensional problem.
- The second point is that in the case of spherically symmetric perturbations ($l = 0$), the perturbed Poisson equation can be integrated, reducing the system to second order for the variables p' and ξ_r . An important consequence, that will not be explored here, is that it is then possible to combine the two first-order differential equations to obtain a single second-order differential equation for the displacement, that can then be cast in the form of a standard wave equation. Moreover, Takata (2005, 2016) has shown that in the case of dipolar modes ($l = 1$), momentum conservation can be used to derive an integral that again reduces the system to second order. In the same work, the author has also argued that integrals such as those found for the case of radial and dipolar modes do not exist for any other mode degree.
- For other mode degrees, reduction of the system of equations (13) to a second order system can be achieved by performing the *Cowling approximation*, which consists in neglecting the perturbation to the gravitational potential. This approximation is adequate for perturbations that vary on relatively short scales (much smaller than the radius of the star). Since the integral solution of the Poisson equation relates ϕ' to the integral of ρ' , the cancellation effect that results from the integration when ρ' varies on short scales, leads to ϕ' being small in that case. While this reduction of the order of the system requires an approximation, it has

proven to be extremely useful for the asymptotic analysis of the equations and, in that way, a better understanding of the physical picture involved. I will get back to this in Sect. 3.

- The fourth, and last point, that should be made is that while the coefficients in the system of equations (13) depend on the mode degree, l , they are independent of the mode azimuthal order, m . This is a consequence of our assumption that the equilibrium state is spherically symmetric. In fact, under that assumption, there is no preferential direction in the star and, so far as the boundary conditions (to be discussed in Sect. 2.4) are also independent of m , the solutions must be independent of the reference about which the spherical harmonic functions are defined. Since m defines the orientation of the spherical harmonic on the sphere, the equations and, hence, the solutions, must not depend on m . This means that under this assumption the solutions will be degenerate in the azimuthal order. That degeneracy, however, is broken (partially broken), in the presence of agents that break (partially break) the spherical symmetry, such as, e.g., rotation or magnetic fields.

2.4 Boundary Conditions

Of the four boundary conditions required to solve the problem set by the system of equations (13), two will be defined at the stellar centre ($r = 0$) and two at the stellar surface ($r = R$).

2.4.1 At the Stellar Centre

The boundary conditions at the stellar centre are derived by imposing that the solutions are regular (do not diverge) there. By expanding the equations near $r = 0$ one finds that the regular solutions require $p' \sim \mathcal{O}(r^l)$, $\phi' \sim \mathcal{O}(r^l)$, and $\xi_r \sim \mathcal{O}(r^\alpha)$, where $\alpha = 1$ for $l = 0$ and $\alpha = l - 1$ for $l > 0$. This means that, as $r \rightarrow 0$,

$$\frac{d\phi'}{dr} - \frac{l}{r}\phi' \rightarrow 0, \quad \frac{dp'}{dr} - \frac{l}{r}p' \rightarrow 0, \quad \frac{d\xi_r}{dr} - \frac{\alpha}{r}\xi_r \rightarrow 0. \quad (15)$$

The three conditions above are not all independent. In fact, the condition on the displacement can be derived from the other two by first noting that the gradient of the thermodynamic variables in the equilibrium structure must be zero at the centre of the star and, then, applying that knowledge to the perturbed equations. Moreover, in that process one also finds that for non-radial modes $\xi_r = l\xi_h$, at $r = 0$. The regularity of the solutions thus provides us with two independent boundary conditions to apply at $r = 0$. One interesting point to notice is that the displacement at the centre of the star is non-zero only for dipolar modes ($l = 1$). In all other cases the centre of the star does not move. That such is the case can also be seen from

symmetry arguments, as only for $l = 1$ modes one would recover the same non-zero displacement vector at $r = 0$ independently from where the centre is approached.

2.4.2 At the Stellar Surface

As the density vanishes outside the star, at the surface the perturbation to the gravitational potential must match continuously onto the physically-meaningful solution of the Poisson equation for a vacuum field (vanishing at infinity). That implies that $\phi' \sim \mathcal{O}(r^{-l-1})$ and thus, at $r = R$,

$$\frac{d\phi'}{dr} = -\frac{l+1}{r}\phi'. \quad (16)$$

The second boundary condition to be applied at the surface depends on how one treats the atmosphere of the star. If one assumes a free boundary, then one must consider that the pressure at the boundary is constant and, hence, that the Lagrangian pressure perturbation there is zero. In that case, a second boundary condition at $r = R$ is found in the form:

$$p' + \frac{dp_0}{dr}\xi_r = 0. \quad (17)$$

This condition is reasonable for low-frequency waves, as will be seen later. However, as the frequency of the waves increases, the details of the atmosphere become more important for the solution. It is therefore common, when solving the pulsation equations, to adopt a more adequate boundary condition, such as that derived from the matching of the radial displacement solution onto the physically meaningful analytical solution derived for an isothermal atmosphere. The analytical solution can be derived assuming a plane-parallel isothermal equilibrium composed of an ideal gas and with constant adiabatic exponent and mean molecular weight. Under these assumptions, the sound speed is constant and so are the density and pressure scale heights, i.e., the characteristic lengths associated with the variations of density and pressure, given respectively by $H = -dr/d \log \rho_0$ and $H_p = -dr/d \log p_0$. Moreover, in this case, the equilibrium pressure and density decrease exponentially with height in the atmosphere $\rho, p \propto \exp[(R - r)/H]$. Then, considering the system of equations (13) under the Cowling approximation, the displacement is found to have the form $\xi_r \propto \exp(\kappa r)$, where, for all cases that will be of interest to us,¹

$$\kappa = \frac{1}{2H} \left[1 \pm \left(1 - \frac{4\omega^2 H^2}{c_0^2} \right)^{1/2} \right] \equiv \frac{1}{2H} \left[1 \pm \left(1 - \frac{\omega^2}{\omega_c^2} \right)^{1/2} \right]. \quad (18)$$

¹Here the term that would dominate in the case of atmospheric gravity waves is being neglected, as those will not be discussed in these lectures.

Combining the perturbed equation of mass conservation and the adiabatic condition (first and fourth equations in the system of Eqs. (10)) with the solution for ξ_r , and noting that in the isothermal atmosphere $H = H_p$, one finds an alternative boundary condition to be applied at $r = R$ [replacing Eq. (17)], namely,

$$p' \approx - \left(\Gamma_{1,0} p_0 \kappa + \frac{dp_0}{dr} \right) \xi_r = \frac{p_0}{H} (1 - \Gamma_{1,0} \kappa H) \xi_r, \quad (19)$$

where $\nabla \cdot \xi$ has been approximated by $d\xi_r/dr$, implicitly assuming that the perturbation varies much more rapidly in the radial than in the horizontal direction.

In Eq. (18) the critical frequency, ω_c , has been introduced, which in the isothermal atmosphere is constant and equal to $c_0/(2H)$. It is important to note that when $\omega < \omega_c$, κ is real and the physically meaningful solution corresponds to choosing the negative sign, ensuring that the energy density, $\propto \rho \xi_r^2$, decreases outwardly. When $\omega > \omega_c$, κ is complex and assuming no waves are being sent into the atmosphere from outside, the imaginary part must be chosen to guarantee that the wave travels outwardly. Considering the time-dependent part of the solution, one finds that the radial component of the displacement goes as $\exp[i(\pm \kappa_i r - \omega t)]$, where $\kappa_i = (\omega^2/\omega_c^2 - 1)^{1/2}$. The outwardly travelling solution is thus obtained by taking the positive sign in Eq. (18).

Under this boundary condition, waves with $\omega > \omega_c$ will simply propagate away, loosing their energy through the boundary.² Here I am interested only in waves that are fully trapped inside the star, loosing no energy through the boundary, hence I will consider only the case when $\omega < \omega_c$. In the particular case when $\omega \ll \omega_c$ the expression for κ can be expanded and the boundary condition [Eq. (19)] approximated by

$$p' = \frac{p_0}{H} \left(1 - \Gamma_1 \frac{\omega^2}{4\omega_c^2} \right) \xi_r. \quad (20)$$

Finally, I note that as the frequency decreases, the second term inside the brackets on the right-hand side of Eq. (20) gets smaller and this boundary condition approaches the one defined in Eq. (17), justifying the adequacy of the latter in the case of sufficiently low frequencies.

2.5 Eigenvalues

The system of equations (13) and associated boundary conditions constitute an eigenvalue problem that needs to be solved numerically. The system admits non-trivial solutions only for discrete values of the eigenvalues ω . The discrete solutions

²In a real stellar atmosphere there can be partial reflection of the wave energy even when $\omega > \omega_c$. Accounting for that would require modifying the atmospheric model and, thus, the outer boundary condition accordingly.

can be associated to an integer number n , denominated by radial order. Once the depth-dependent amplitudes of the perturbations are computed, the full solutions can be derived from Eq. (11).

In summary, the eigenvalues, $\omega = \omega(n, l, m)$, of the 3-dimensional problem set by the pulsation equations (10) (after separation of time) are characterized by three quantum numbers, n , l , and m , where the absolute value of the first, $|n|$, is related to the number of nodes of the perturbation along the radial direction, while the other two, introduced in Sect. 2.3, are related to the angular dependence of the solutions, in particular to the horizontal scale of the perturbation and its orientation on the stellar surface. The discrete nature of the eigenvalues is clearly seen in the power density spectrum of the Sun shown in Fig. 1.

As discussed before, in the absence of physical agents that break the spherical symmetry of the problem, the solutions must be degenerate in m . Hence, in that case one has $\omega = \omega(n, l)$ and any linear combination of the $2l + 1$ independent solutions associated with the spherical harmonic of degree l , and different m values, is still an eigensolution for that eigenvalue.

A discussion of the full solutions obtained from numerical integration of the pulsation equations will be presented in Sect. 4. First, however, it is useful to analyse the second-order equation that is derived from the system of equations (13) under particular approximations. That will be discussed in the next section.

3 Trapping of the Oscillations

The full solutions of the linear, adiabatic pulsation equations must be computed numerically. Nevertheless, under the Cowling approximation, valid for large absolute values of the radial order, $|n|$, or for large degree l , the system of equations (13) reduces to second order on the variables p' and ξ_r , namely,

$$\begin{aligned} \frac{1}{r^2} \frac{d}{dr} (r^2 \xi_r) - \frac{g_0}{c_0^2} \xi_r - \left(\frac{S_l^2}{\omega^2} - 1 \right) \frac{1}{c_0^2 \rho_0} p' &= 0, \\ \frac{dp'}{dr} + \frac{g_0}{c_0^2} p' - \rho_0 (\omega^2 - N_0^2) \xi_r &= 0. \end{aligned} \quad (21)$$

These equations can be combined to find a second-order wave equation for a single variable. To do so, I follow the work of Deubner and Gough (1984), which, in addition to the Cowling approximation, assumes that locally the oscillations can be treated as in a plane-parallel layer under constant gravity, hence neglecting³ the derivatives of r and g_0 . Let us introduce a new variable,

$$\Psi = \rho_0^{1/2} c_0^2 \nabla \cdot \xi, \quad (22)$$

³For a more general case in which these assumptions are not made, see Gough (1993).

which through the adiabatic condition and the continuity equation can be seen to be directly related to the Lagrangian pressure perturbation ($\delta p = -\rho_0^{1/2}\Psi$). The second-order system (21), under the approximations mentioned above, can be manipulated to derive a wave equation for Ψ ,

$$\frac{d^2\Psi}{dr^2} + \kappa_r^2\Psi = 0, \quad (23)$$

where κ_r is the local radial wavenumber given by

$$\kappa_r^2 = \frac{1}{c_0^2} \left[S_l^2 \left(\frac{N_0^2}{\omega^2} - 1 \right) + \omega^2 - \omega_c^2 \right], \quad (24)$$

and the critical frequency is now given by

$$\omega_c^2 = \frac{c_0^2}{4H^2} \left(1 - 2 \frac{dH}{dr} \right). \quad (25)$$

Notably, k_r depends critically on the three characteristic frequencies introduced before, namely, S_l , N_0 and ω_c . Examples of ω_c for a solar model and a red-giant model are shown in Figs. 4 and 5, respectively. It is small in the stellar interior, where the density varies on large scales, but it becomes large near the surface, where structural variations take place on a much shorter scale.

3.1 Mode Propagation Cavities

If κ_r^2 were constant and positive, the solution would be oscillatory everywhere. However, in a star κ_r^2 is a function of r , and one may generally expect it to be positive in some region(s) and negative in others. Where it is positive, the solution is locally wave-like (oscillatory in r) while where it is negative it is locally exponential. Because κ_r^2 depends on ω , the regions where wave-like solutions are found will depend on the mode under consideration. When there is only one region of the star where $\kappa_r^2 > 0$, the mode is said to be trapped there and that region is often called the mode propagation cavity. Away from that cavity, where the energy of the mode decreases exponentially, the mode is said to be evanescent. When κ_r^2 is positive in more than one region of the star, separated by regions where it is negative, the mode propagates in more than one cavity. However, often most of its energy is concentrated in one of these cavities whose structure, in turn, is the most determinant for the properties of the mode.

The radii at which $\kappa_r^2 = 0$ are called the turning points and define the edges of the propagation cavities. Setting the left-hand side of Eq. (24) to zero, one finds a second-order algebraic equation for ω^2 , whose roots, $\omega_{l,\pm}^2$, are given by

$$\omega_{l,\pm}^2 = \frac{1}{2} (S_l^2 + \omega_c^2) \pm \frac{1}{2} \sqrt{(S_l^2 + \omega_c^2)^2 - 4S_l^2 N_0^2}, \quad (26)$$

where the index l was used to recall that the roots depend on the mode degree through their dependence on the Lamb frequency. Rewriting Eq. (24) as

$$\kappa_r^2 = \frac{1}{c_0^2} [\omega^2 - \omega_{l,+}^2] [\omega^2 - \omega_{l,-}^2] , \quad (27)$$

one sees that modes propagate if

$$\omega > \omega_{l,+} \quad \text{or} \quad \omega < \omega_{l,-} , \quad (28)$$

and modes are evanescent if

$$\omega_{l,-} < \omega < \omega_{l,+} . \quad (29)$$

Figure 6 shows the frequencies $\omega_{l,\pm}$ for a model of the Sun in what is usually called a propagation diagram. Comparison with Fig. 4 shows the resemblance between N_0 and $\omega_{l,-}$. The frequency $\omega_{l,+}$, on the other hand, resembles S_l in the deeper layers of the stellar model, but it is clearly dominated by ω_c in the outer layers. Three modes, two at high frequency and one at low frequency, are illustrated by the horizontal lines in Fig. 6. For each of these modes, the propagation cavity

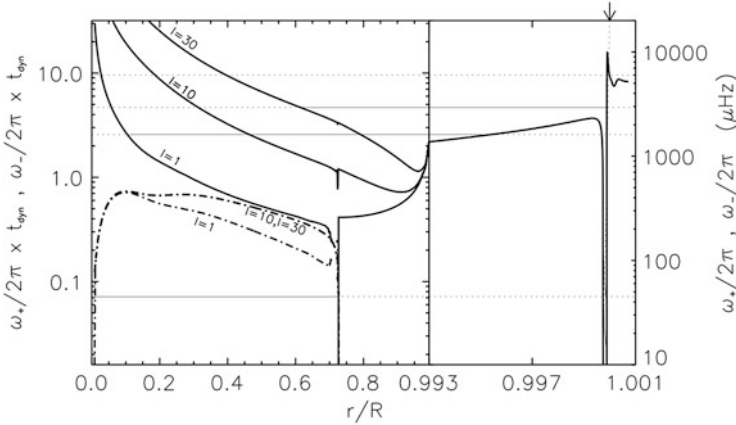


Fig. 6 Propagation diagram for model S of the Sun (Christensen-Dalsgaard et al. 1996). The frequencies ω_+ (continuous thick lines) and ω_- (shaded-dotted thick lines) are shown for three different values of mode degree, l . Note that in the outer layers (right-hand section of the plot), the horizontal axis varies much slower than in the inner layers (left-hand section of the plot). The arrow at the top marks $r/R = 1$. The horizontal lines mark four different frequencies and are continuous where the mode is trapped. At the lowest end, we have a characteristic g-mode frequency for this model, with $\nu \sim 45 \mu\text{Hz}$. At the highest end we have a frequency $\nu \sim 6000 \mu\text{Hz}$ that is too high to be trapped inside the star. In between, we have two p-modes, one with $l = 1$, $\nu \approx 1613 \mu\text{Hz}$, and one with $l = 30$, $\nu \approx 2936 \mu\text{Hz}$. The left-hand side vertical axis shows the range of values taken by these frequencies when they are scaled according to their dependence on the dynamical timescale, while the right-hand side axis shows their true physical values

corresponds to the section in which the horizontal line is continuous. A fourth frequency is marked, with $\nu \sim 6000 \mu\text{Hz}$, which is too high to correspond to a trapped mode.

3.2 Acoustic Versus Internal Gravity Waves

Inspection of the propagation diagram shown in Fig. 6 points towards the existence of two families of solutions, one at lower frequencies, where the mode cavity is essentially determined by the buoyancy frequency, and one at higher frequencies, where the propagation cavity is determined by the combination of the Lamb frequency, in the deeper regions, and the critical frequency, near the surface. This can also be seen by considering the lower and higher frequency limits of κ_r^2 in the propagation region, as discussed below.

3.2.1 Acoustic Waves

Let us consider first the higher frequency limit, namely, the case when $\omega^2 \gg N_0^2$, in regions where $\kappa_r^2 > 0$. Except near the surface, where ω_c becomes large, Eq. (24) then gives

$$\kappa_r^2 \approx \frac{\omega^2}{c_0^2} - \frac{l(l+1)}{r^2}. \quad (30)$$

Recalling that the last term on the right-hand side is κ_h^2 [cf. Eq. (12)], one finds that

$$|\kappa|^2 \equiv \kappa_r^2 + \kappa_h^2 \approx \frac{\omega^2}{c_0^2}. \quad (31)$$

One thus has, for $\omega^2 \gg N_0^2$, a dispersion relation of the type:

$$\omega \approx c_0 |\kappa|, \quad (32)$$

which is characteristic of acoustic waves. These waves are maintained by the gradient of the pressure perturbation, i.e., the first term on the right-hand side of the perturbed momentum equation. Note that in this case the frequency of the mode increases as κ increases. Taking the radial order for this family of solutions as being positive integers, n , one thus finds that the frequency of acoustic modes increases both with increasing radial order, n , and with increasing degree, l .

Looking back at Eq. (30), one can further establish the lower turning point for the acoustic modes, that defines the lower boundary of their propagation cavity. Setting

κ_r^2 to zero implies $\omega^2 = S_l^2$, from which the lower turning point is found to be defined by

$$r_{1,l} = \frac{\sqrt{l(l+1)}c_0(r_{1,l})}{\omega}, \quad (33)$$

where the subscript l has been used to emphasize that the lower turning point depends on the mode degree and it has been explicitly indicated that the value of c_0 is to be taken at the turning point. From Eq. (33), we see that the lower turning point of acoustic modes depends strongly on the mode degree. As the mode degree increases, the lower turning point gets closer to the surface, implying that the propagation cavity of the mode becomes shallower. That is also evident in Fig. 6, where one can see that the depth at which a horizontal line in the high-frequency regime crosses lines of $\omega_{l,+}$ for different degrees, becomes smaller as the degree increases. In addition, we see from Eq. (33), and also from inspection of Fig. 6, that for a fixed mode degree, the lower turning point decreases as the mode frequency increases. That means that higher frequency acoustic modes propagate deeper, for fixed mode degree.

The upper turning point of the acoustic modes is, in turn, determined by comparing the oscillation frequency with the critical frequency, which near the surface is much greater than S_l . There, one may approximate,

$$\kappa_r^2 \approx \frac{\omega^2 - \omega_c^2}{c_0^2}. \quad (34)$$

Thus, one finds that $\kappa_r = 0$ in the outer layers if

$$\frac{c_0}{2H} \left[1 - 2 \frac{dH}{dr} \right]^{1/2} \approx \omega, \quad (35)$$

which provides an implicit condition for the upper turning point of acoustic modes, r_2 . Note that unlike the case of the lower turning point, to this approximation the upper turning point of acoustic modes is independent of the mode degree.

The upper turning point of acoustic modes in a solar-like model is best seen in the right-hand section of Fig. 6. For the lowest of the three frequencies in the high-frequency regime ($\nu \approx 1613 \mu\text{Hz}$), the upper turning point is below the photosphere, while for the second lowest ($\nu \approx 2936 \mu\text{Hz}$) it is at the photosphere. For that reason, the former is significantly less sensitive to the details of the outer layers than the latter. This is relevant because these layers are particularly difficult to model. The oscillation frequencies derived from models are therefore affected by the incomplete modelling of the outer layers and, as a result, show systematic differences when compared with the observations. This is less so for the lower frequency acoustic modes, which may, in that case, serve as an anchor with which to get a handle on the systematic errors (assuming some kind of frequency dependence

of these errors). The other point to notice is that there is a frequency above which no trapping is possible. This has been discussed in Sect. 2.4.2, where the critical frequency for a plane-parallel, ideal, isothermal atmosphere has been introduced. Independently of taking the latter, or the more realistic critical frequency shown in Fig. 6, it is clear that above ~ 5.3 mHz full trapping of the modes no longer occurs. Since ω_c also scales with the inverse of the dynamical timescale (as seen when comparing Figs. 4 and 5), the maximum expected observed frequency is strongly dependent on the evolutionary state of the star.

3.2.2 Internal Gravity Waves

Let us now turn our attention to the low frequency limit of Eq. (24) in regions where $\kappa_r^2 > 0$. Let us consider that $\omega^2 \ll S_l^2$ throughout that propagation region and, in addition, that $\omega_c^2 \ll S_l^2$ there. In that case k_r^2 is given approximately by

$$\kappa_r^2 \approx \frac{S_l^2}{c_0^2 \omega^2} [N_0^2 - \omega^2]. \quad (36)$$

Recalling that $\kappa_h^2 = l(l+1)/r^2 = S_l^2/c_0^2$, we then find the dispersion relation

$$\omega^2 \approx \frac{N_0^2}{1 + k_r^2/\kappa_h^2}, \quad (37)$$

which is characteristic of internal gravity waves. Internal gravity waves are maintained by the gravity acting on the perturbation to the density. If one considers a slow upwards displacement of an element of fluid whose pressure is kept in equilibrium with the surrounding, buoyancy will respond to restore the fluid towards the equilibrium position if its density is larger than that of the surroundings. That, in turn, can lead to the oscillatory motion associated to gravity waves. Because an element of fluid cannot move strictly vertically, there is always an horizontal component of the motion, which, in turn, means that gravity waves can never be associated to spherically symmetric perturbations, i.e., there are no gravity waves of degree $l = 0$. Moreover, since buoyancy will only oppose to the motion of the element of fluid where $N_0^2 > 0$, i.e., in convectively stable regions, the gravity waves will only propagate where there is no convection.

Looking back at the dispersion relation in Eq. (37), there are additional points that should be noted. First, the frequency of gravity waves is always smaller than N_0 . This just confirms the role of buoyancy in maintaining the dynamics of gravity waves. The second point is that the frequency of gravity waves depends critically on the shape of the perturbation. In fact, when the perturbation is “needle-like”, meaning that $K_r^2/K_h^2 \ll 1$, the frequency is higher, tending to N_0 as that ratio tends to zero. In the other limit, for wide perturbations with $K_r^2/K_h^2 \gg 1$, the oscillation frequency is smaller, tending to zero as the ratio becomes increasingly higher. This

can be understood if we recall that the amount of material displaced horizontally is larger in the latter case than in the former. This horizontal displacement, and the horizontal pressure gradient that it originates, increases the effective inertia of the element of fluid on which the buoyancy force is acting. The result is a smaller acceleration of the element of fluid and, consequently, a smaller mode frequency.

It is worth emphasizing that the aspects discussed above are in striking contrast with what was previously found for acoustic waves. Indeed, for acoustic waves the frequency is found to depend essentially on the characteristic scale of the perturbation, determined by the total wavenumber $|\kappa|$, while for gravity waves the frequency depends in addition, and very critically, on the relation between the horizontal and vertical scales. Moreover, considering modes of a given degree (hence fixing the horizontal scale), we find that the frequency of gravity waves decreases with increasing κ_r . Taking the radial orders n as negative integers, as is commonly done for gravity waves, we see that their frequencies decrease with increasing $|n|$, again in contrast with what was found earlier for acoustic waves.

Finally, from Eq. (36) we find that under the conditions assumed, gravity waves propagate between the radii at which $N_0 = \omega$. The latter thus provides an implicit condition for the lower and upper turning points of these modes which to this approximation are independent of the mode degree, l . This is, again, in contrast with the case of acoustic modes, for which the lower turning point, and, hence, the extent of the propagation cavity, was found to be strongly dependent on the mode degree. For the case of a star like the Sun, we see from Fig. 6 that the lower frequency gravity modes are essentially trapped between the centre of the star and the base of the convective region. For the highest frequency gravity modes the upper turning point gets smaller and the modes are trapped in deeper layers. For main-sequence stars more massive than the Sun, the innermost layers are convectively unstable and, thus, the cavity of gravity waves is bounded on the inner side by the edge of the convectively unstable core. On the other hand, since the convective envelope gets shallower for more massive stars, gravity waves there can propagate almost to the stellar surface. In more evolved stars, the trapping region again depends on the existence, or not, of convection in the core, as well as on the extent of the convective envelope, which can get very deep, as happens, for instance, along the red-giant branch. Moreover, the steep increase of the buoyancy frequency in the core of evolved stars, such as that shown in Fig. 5, can lead to several cavities of propagation for the same mode, in which case the analysis becomes more complex than in the cases discussed above. I will get back to that case in the next section, where the full numerical results of the pulsation equations shall be discussed. Table 1 provides a summary of the properties of acoustic and gravity waves.

3.3 The Surface Gravity Waves

For completeness, in this section I will consider the case of perturbations obeying $\delta p = 0$, hence, $\Psi = 0$. Going back to the system of equations (21), and considering,

Table 1 Summary of the properties of acoustic and gravity waves discussed in this chapter

| Acoustic waves | Gravity waves |
|--|---|
| Maintained by the gradient of pressure fluctuation | Maintained by gravity acting on density fluctuation |
| Radial or non-radial | Always non-radial |
| Propagate in convectively stable or unstable regions | Propagate in convectively stable regions only |
| Propagation cavity strongly dependent on l | Propagation cavity largely independent of l |
| Frequency increases with increasing n and increasing l | Frequency always $< \max(N_0)$. It increases with increasing l , and decreases with increasing $ n $ |

as before, that locally the oscillations can be treated as in a plane-parallel layer under constant gravity, we find:

$$\begin{aligned}
 \frac{d\xi_r}{dr} - \frac{g_0\kappa_h^2}{\omega^2}\xi_r + \frac{1}{\rho_0 c_0^2} \left(1 - \frac{c_0^2\kappa_h^2}{\omega^2}\right) \delta p &= 0, \\
 \frac{d\delta p}{dr} + \frac{g_0\kappa_h^2}{\omega^2}\delta p - \rho_0 g_0 \left(\frac{\omega^2}{g_0} - \frac{g_0\kappa_h^2}{\omega^2}\right) \xi_r &= 0.
 \end{aligned} \tag{38}$$

For $\delta p = 0$, the system above is satisfied by an exponential solution of the type $\xi_r = \exp[\kappa_h(r - r_0)]$, where $\kappa_h = \omega^2/g_0$. Here, r_0 is a fiducial depth in the vicinity of which the plane-parallel approximation is being made and g_0 is the gravitational acceleration at $r = r_0$. Thus, the depth-dependent amplitude of the solution in this case decays exponentially with depth and the dispersion relation is $\omega = \sqrt{g_0\kappa_h}$. Moreover, under the approximations considered here, it is independent of the stratification of the star. Since the characteristic scale of the amplitude decay is κ_h^{-1} , the plane-parallel approximation is particularly adequate when κ_h , hence the degree l of the mode, is not too small and the mode is concentrated near the surface of the star.

This solution can be identified as a surface gravity wave, similar to a wave propagating at the surface of a deep ocean. Since $\delta p = 0$, $\nabla \cdot \xi = 0$ and the fluid is not compressed during the perturbation.

4 Numerical Solutions to the Pulsation Equations

The full solutions to the pulsation equations and associated boundary conditions must be computed numerically. In this section, I briefly discuss the range of solutions obtained for a model of the Sun and discuss also a specific example for a star in a different evolutionary state.

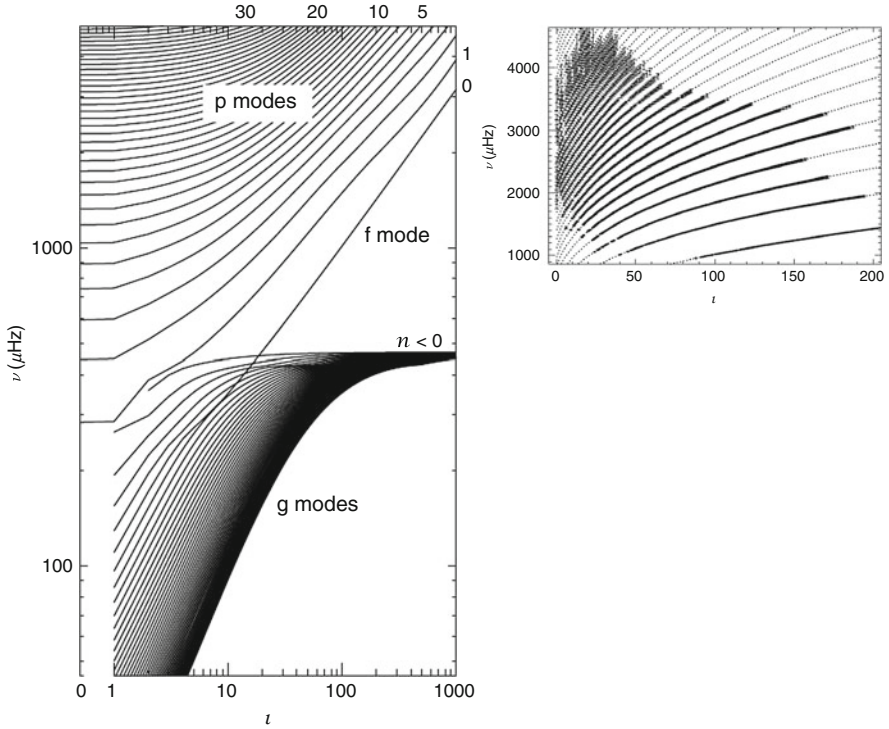


Fig. 7 *Left:* Cyclic frequencies computed for a model of the Sun, as function of mode degree, l . The discrete eigenvalues for each radial order have been joined by *continuous lines* with a few examples of the radial order identified on the right-hand side and top of the figure. *Right:* Frequencies of the Sun derived from 144 days of observations with the instrument MDI on board the *SOHO* spacecraft. The depicted error bars correspond to 1000σ . The *dotted lines* show the model results, for comparison. Figure adapted from Christensen-Dalsgaard (2008c) and Aerts et al. (2010)

The left panel of Fig. 7, adapted from Aerts et al. (2010), shows the cyclic frequencies ($=\omega/2\pi$) computed with the Aarhus adiabatic oscillation package (ADIPLS; Christensen-Dalsgaard 2008a) for a solar model obtained with the Aarhus STellar Evolution Code (ASTEC; Christensen-Dalsgaard 2008b). The discrete eigenvalues for each radial order have been joined by continuous lines with a few examples of the radial order identified on the right-hand side and top of the figure. Three families of solutions are identified in the figure: (1) The acoustic (or p-) modes, at higher frequencies; (2) the gravity (or g-) modes, at lower frequencies, and; (3) the f-mode, at intermediate frequencies. These correspond to the cases discussed in the previous section, based on the analysis under the Cowling approximation. For comparison, the eigenfrequencies of the real Sun, derived from data acquired with the instrument MDI on board of the *SOHO* spacecraft are shown on the right panel of the same figure, where the model results are overplotted

as dotted curves. Only the p- and f-modes are seen in the real data. In fact, the observation of gravity modes in the Sun has been a long-standing goal, but despite all efforts and some claims of detection of signatures of g-modes and, possibly, individual g-modes in the Sun (García et al. 2007; García 2010), the matter is still not settled (Appourchaux et al. 2010).

A closer look at the different families of solutions displayed in Fig. 7 shows that the behaviour of the solutions with changing radial order and mode degree also follows what was found from the analysis in Sect. 3. For the p-modes, at fixed degree, l , we can see an increase of the frequency with radial order. Likewise, following a single line of fixed radial order, n , we also see an increase of the frequency with increasing degree. Both of these dependencies were expected from the dispersion relation for acoustic waves derived earlier. Regarding the g-modes, we can identify an upper bound to the frequency, which corresponds to the maximum value of the buoyancy frequency in that model. In addition, I note that there are no results for spherically symmetric modes, $l = 0$, as expected given that the displacement associated with these waves can never be purely radial (always involves a horizontal displacement of the fluid). Moreover, it is seen that at fixed degree the frequency decreases with increasing absolute value of the radial order, $|n|$, while at fixed radial order, the frequency increases with increasing degree. I also note that the fact that the lines of g-mode solutions are very close to each other implies that at fixed frequency the radial order increases very rapidly with increasing mode degree. As for the case of p-modes, the numerical results discussed here are in agreement with the dispersion relation for g-modes derived in Sect. 3. Finally, the f-mode eigenfrequencies for moderate to high mode degrees (the ones for which the plane-parallel approximation used in Sect. 3 is adequate), are found between the p-mode and g-mode eigenfrequencies. Despite the resemblance of the high degree f-mode solutions and the p-mode solutions I wish to recall that these modes obey $\delta p = 0$. Thus, the perturbation takes place without compression or refraction of the fluid, reminding us that f-modes are not acoustic waves.

The trapping of the modes discussed in Sect. 3 can also be verified by inspection of the numerical eigenfunctions. In Fig. 8 three examples of p-mode (left panel) and g-mode (right panel) eigenfunctions are shown, for the solar model discussed above. The quantity plotted, $r^3 \delta p$, has the dimensions of energy and, in each case, it is normalized to its maximum value. Inspection of the p-mode solutions shows that the spherically symmetric pulsation ($l = 0$; top panel) propagates from the centre to the stellar surface. One may then expect it to carry average information about the entire star. In contrast, a p-mode of similar frequency but much higher degree ($l = 60$; bottom panel) has its energy concentrated in the outer layers of the star. This was expected from the analysis performed in Sect. 3, where it was found that the propagation cavity of p-modes becomes shallower as the mode degree increases. Looking now at the right panel we see that, in contrast with the p-modes, the energy of the g-modes is concentrated towards the innermost layers of the star. The modes are trapped below the convective envelope (marked by the vertical dotted line), in a cavity that is mostly independent of mode degree. The modes shown have similar frequency, so as anticipated from Fig. 7, even a small increase in mode degree results

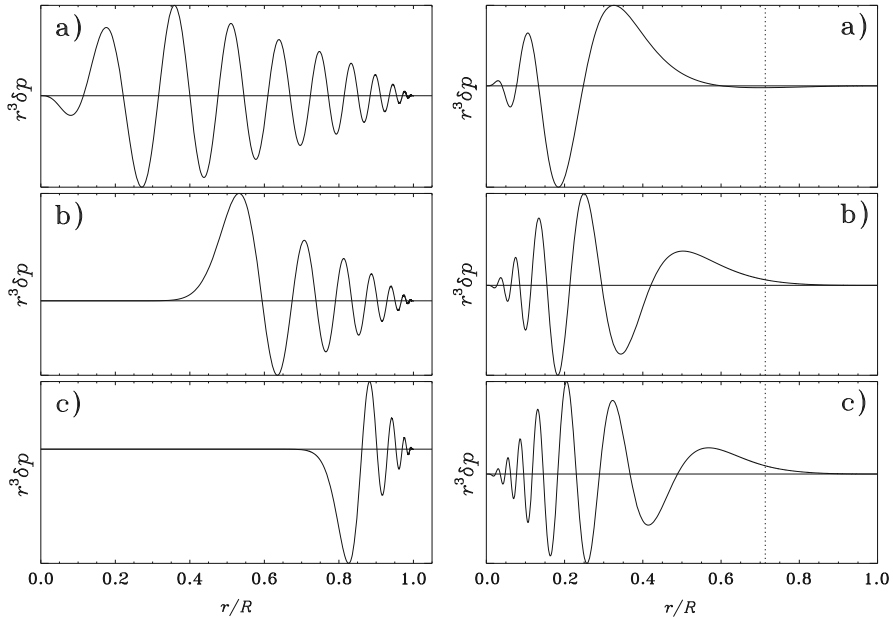


Fig. 8 Normalized eigenfunctions for a model of the Sun, as function of fractional radius. The chosen eigenfunction, $r^3 \delta p$, has the dimensions of energy and is normalized to its maximum value. *Left:* Results for three p-modes: (a) ($l = 0, n = 21, \nu = 3038.0 \mu\text{Hz}$), (b) ($l = 20, n = 14, \nu = 2939.2 \mu\text{Hz}$), and (c) ($l = 60, n = 9, \nu = 3043.2 \mu\text{Hz}$). *Right:* Results for three g-modes: (a) ($l = 1, n = -5, \nu = 109.2 \mu\text{Hz}$), (b) ($l = 2, n = -10, \nu = 102.6 \mu\text{Hz}$), and (c) ($l = 3, n = -14, \nu = 104.1 \mu\text{Hz}$). The dotted line marks the base of the convective envelope (figure courtesy of J. Christensen-Dalsgaard)

is a significant increase in the radial order, as seen from the increase in the number of nodes when comparing the upper and lower panels on the right-hand side.

The regions where modes propagate depend directly on the stellar structure and, hence, are different for stars of different masses or different evolutionary states. In Sect. 2.3 I have pointed out that as the star evolves beyond the main sequence, and the core contracts, the buoyancy frequency increases significantly towards the centre. This results in the appearance of mixed modes, i.e., modes that are maintained by gravity acting on density perturbations in the deep interior, and by the gradient of the pressure perturbation in the outer layers. An example of such a mode computed for the model shown in Fig. 5 is shown in Fig. 9. Two mode cavities can be identified, in the inner and outer layers of the star, respectively, separated by an evanescent region where the solution is not oscillatory. Despite the latter, coupling does exist between the two cavities and in a general case the solution is different from what would be found if the two cavities were considered independently of each other.

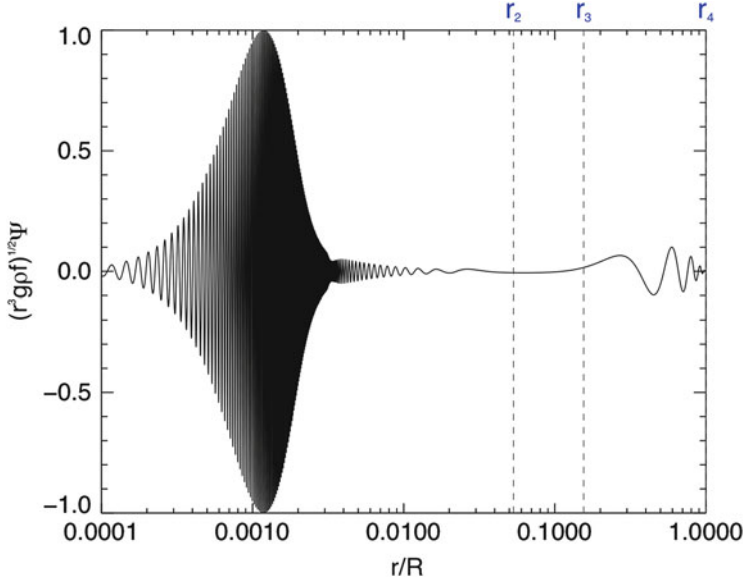


Fig. 9 Same as Fig. 8, for a dipole mode with frequency $\nu = 51.20 \mu\text{Hz}$, in a model of a star in the red-giant branch. The *vertical, dashed lines* show the position of the two turning points bounding the evanescent region, namely, r_2 and r_3 . The outermost turning point, r_4 , is also shown, while the innermost turning point, r_1 , is outside the plotted range. The g-mode cavity is located between the unseen r_1 and r_2 , and the p-mode cavity is located between r_3 and r_4 . Figure adapted from Cunha et al. (2015)

5 Discussion

As mentioned from the outset, a number of aspects of the theory of stellar pulsations had to be left out of these notes in the interest of space. In what follows, I identify issues that I find particularly important and that are discussed in detail in the books and lecture notes mentioned in the introduction.

To start with, it should be pointed out that it is possible to perform an asymptotic analysis of the second-order pulsation equations derived under the Cowling approximation to find approximate eigenvalues and eigenfunctions for modes of high radial orders and low degree. That has been performed in different ways by different authors (Vandakurov 1968; Tassoul 1980; Unno et al. 1989; Gough 1993). In the case of p-modes, the eigenfrequencies in this limit are found to be well approximated by

$$\nu_{nl} \simeq \left(n + \frac{l}{2} + \frac{1}{4} + \alpha \right) \Delta \nu_0 - [Al(l+1) - \delta] \frac{\Delta \nu_0^2}{\nu_{nl}}, \quad (39)$$

where

$$\Delta v_0 = \left(2 \int_0^R \frac{dr}{c} \right)^{-1} \quad (40)$$

is the inverse sound travel time across a stellar diameter, and

$$A = \frac{1}{4\pi^2 \Delta v_0} \left[\frac{c(R)}{R} - \int_0^R \frac{dc}{dr} \frac{dr}{r} \right]. \quad (41)$$

Here, α is a slowly varying function of frequency determined by the reflection properties near the surface and δ is a small correction term predominantly related to the near-surface region. To leading order, Eq. (39) predicts the uniform spacing between frequencies of consecutive modes of the same degree, corresponding to the large frequency separation, Δv , observed in Fig. 1. Also, we see that modes of odd degree fall halfway between modes of even degree. The first term in Eq. (39) cancels out when subtracting the frequencies of modes of consecutive orders and degrees differing by two. That combination then gives the small frequency separation, δv , also seen in Fig. 1, and which is found to be

$$\delta v_{nl} = v_{nl} - v_{n-1, l+2} \simeq -(4l+6) \frac{\Delta v_0}{4\pi^2 v_{nl}} \int_0^R \frac{dc}{dr} \frac{dr}{r}, \quad (42)$$

where the small term $c(R)$ in Eq. (41) has been neglected. From Eq. (42) we see that the small separation is particularly sensitive to the innermost layers, as a result of the r^{-1} dependence of the integrand. Other small separations and ratios of small to large separations are often considered in asteroseismology. In particular, the ratios (Roxburgh and Vorontsov 2003; Cunha and Metcalfe 2007) have the advantage that they are essentially independent of the inadequately modelled surface layers of the stars.

In the case of high radial order, low-degree g-modes, the first-order term of the asymptotic analysis predicts a uniform spacing in mode period, Π_{nl} , rather than in frequency. In this case, we have (e.g., Tassoul 1980; Smeyers and Moya 2007):

$$\Pi_{nl} \simeq \frac{\Pi_0}{\sqrt{l(l+1)}} (n + \alpha_{l,g}), \quad (43)$$

where

$$\Pi_0 = 2\pi^2 \left(\int_{r_1}^{r_2} N \frac{dr}{r} \right)^{-1}. \quad (44)$$

The phase $\alpha_{l,g}$ depends on whether the core of the star is radiative or convective, depending on mode degree in the first case but not in the latter. In the case of a radiative core one can write $\alpha_{l,g} = l/2 + \alpha_g$, where α_g is independent of mode

degree. Note, however, that in both cases there is a strong dependence on mode degree of the period spacings between modes of the same degree and consecutive orders, due to the term $[l(l+1)]^{-1/2}$ in Eq. (43). This is in contrast with the case of p-modes for which the asymptotic large separation is, to first order, independent of mode degree.

Another important aspect that has been left out of this chapter is the impact on the oscillation spectrum of rotation and magnetic fields. A perturbative analysis of the impact of rotation on pulsations can be found, e.g., in Aerts et al. (2010), while the impact of an internal magnetic field can be found, e.g., in Gough (1993). Non-perturbative analyses of these phenomena, required in the cases of fast rotation or magnetic fields that permeate the stellar surface, are discussed by Lignières et al. (2006), Reese et al. (2006) and Cunha and Gough (2000), Cunha (2006), respectively.

The ultimate goal of stellar pulsations studies is to infer information about the physics and dynamics of stellar interiors from the asteroseismic data. That is commonly achieved through forward modelling, a method that is intrinsically model-dependent, or, in optimal cases, through inverse techniques, in which the solutions are not restricted to those of a set of models.

Finally, I note that no word has been said about the driving of the pulsations, with the exception of a brief reference, in Sect. 1, to the fact that modes can be intrinsically stable, as in solar-like pulsators, or unstable, as in classical pulsators. This topic is, however, well out of the scope of the present notes and I, thus, refer the interested reader to the literature listed in Sect. 1, and references therein.

Acknowledgements I am grateful to Ângela Santos for producing Fig. 1 and to Jørgen Christensen-Dalsgaard for producing Fig. 8. This work was supported by Fundação para a Ciência e a Tecnologia (FCT) through national funds (UID/FIS/04434/2013) and by FEDER through COMPETE2020 (POCI-01-0145-FEDER-007672), as well as through the Investigador FCT Contract No. IF/00894/2012/CP0150/CT0004. This work has received funding from EC, under FP7, through the grant agreement FP7-SPACE-2012-312844.

References

- Aerts, C., Christensen-Dalsgaard, J., Kurtz, D.W.: *Asteroseismology*. Springer, Berlin (2010)
- Appourchaux, T., Belkacem, K., Broomhall, A.-M., et al.: *Astron. Astrophys. Rev.* **18**, 197 (2010)
- Baglin, A., Auvergne, M., Barge, P., et al.: In: Fridlund, M., Baglin, A., Lochard, J., Conroy, L. (eds.) *The CoRoT Mission Pre-Launch Status - Stellar Seismology and Planet Finding*, vol. 1306, p. 33. ESA Special Publication, Noordwijk (2006)
- Basu, S.: *Living Rev. Sol. Phys.* **13**, 2 (2016)
- Brown, T.M., Gilliland, R.L., Noyes, R.W., Ramsey, L.W.: *Astrophys. J.* **368**, 599 (1991)
- Christensen-Dalsgaard, J.: *Astrophys. Space Sci.* **316**, 113 (2008a)
- Christensen-Dalsgaard, J.: *Astrophys. Space Sci.* **316**, 13 (2008b)
- Christensen-Dalsgaard, J.: The art of modeling stars in the 21st century. In: Deng, L., Chan, K.L. (eds.) *IAU Symposium*, vol. 252, pp. 135–147 (2008c)
- Christensen-Dalsgaard, J., Dappen, W., Ajukov, S.V., et al.: *Science* **272**, 1286 (1996)
- Cunha, M.S.: *Mon. Not. R. Astron. Soc.* **365**, 153 (2006)

- Cunha, M.S., Gough, D.: *Mon. Not. R. Astron. Soc.* **319**, 1020 (2000)
- Cunha, M.S., Metcalfe, T.S.: *Astrophys. J.* **666**, 413 (2007)
- Cunha, M.S., Aerts, C., Christensen-Dalsgaard, J., et al.: *Astron. Astrophys. Rev.* **14**, 217 (2007)
- Cunha, M.S., Stello, D., Avelino, P.P., Christensen-Dalsgaard, J., Townsend, R.H.D.: *Astrophys. J.* **805**, 127 (2015)
- Deubner, F.-L., Gough, D.: *Annu. Rev. Astron. Astrophys.* **22**, 593 (1984)
- Domingo, V., Fleck, B., Poland, A.I.: *Sol. Phys.* **162**, 1 (1995)
- Fröhlich, C., Romero, J., Roth, H., et al.: *Sol. Phys.* **162**, 101 (1995)
- García, R.A.: *Highlights Astron.* **15**, 345 (2010)
- García, R.A., Turck-Chièze, S., Jiménez-Reyes, S.J., et al.: *Science* **316**, 1591 (2007)
- Gilliland, R.L., Brown, T.M., Christensen-Dalsgaard, J., et al.: *Publ. Astron. Soc. Pac.* **122**, 131 (2010)
- Gough, D.O.: In: Zahn, J.-P., Zinn-Justin, J. (eds.) *Astrophysical Fluid Dynamics - Les Houches 1987*, pp. 399–560 (1993)
- Jiménez, A., Roca Cortés, T., Jiménez-Reyes, S.J.: *Sol. Phys.* **209**, 247 (2002)
- Kjeldsen, H., Bedding, T.R.: *Astron. Astrophys.* **293**, 87 (1995)
- Koch, D.G., Borucki, W.J., Basri, G., et al.: *Astrophys. J. Lett.* **713**, L79 (2010)
- Lignières, F., Rieutord, M., Reese, D.: *Astron. Astrophys.* **455**, 607 (2006)
- Reese, D., Lignières, F., Rieutord, M.: *Astron. Astrophys.* **455**, 621 (2006)
- Roxburgh, I.W., Vorontsov, S.V.: *Astron. Astrophys.* **411**, 215 (2003)
- Smeyers, P., Moya, A.: *Astron. Astrophys.* **465**, 509 (2007)
- Takata, M.: *Publ. Astron. Soc. Jpn.* **57**, 375 (2005)
- Takata, M.: *Publ. Astron. Soc. Jpn.* **68**, 109 (2016)
- Tassoul, M.: *Astrophys. J. Suppl. Ser.* **43**, 469 (1980)
- Unno, W., Osaki, Y., Ando, H., Saio, H., Shibahashi, H.: *Nonradial Oscillations of Stars*. University of Tokyo Press, Tokyo (1989)
- Vandakurov, Y.V.: *Sov. Astron.* **11**, 630 (1968)
- Verner, G.A., Elsworth, Y., Chaplin, W.J., et al.: *Mon. Not. R. Astron. Soc.* **415**, 3539 (2011)

Asteroseismology and Exoplanets: Listening to the
Stars and Searching for New Worlds
IVth Azores International Advanced School in Space
Sciences

Campante, T.; Santos, N.; Monteiro, M.J.P.F.G. (Eds.)
2018, XVI, 282 p. 74 illus., 53 illus. in color., Hardcover
ISBN: 978-3-319-59314-2